



High-Throughput and Data Driven Strategies for the Design of Deep-Eutectic Solvent Electrolytes

Journal:	<i>Molecular Systems Design & Engineering</i>
Manuscript ID	ME-ART-03-2022-000050.R2
Article Type:	Paper
Date Submitted by the Author:	12-May-2022
Complete List of Authors:	Rodriguez, Jaime; University of Washington, Chemical Engineering Politi, Maria; University of Washington, Chemical Engineering Adler, Stuart; University of Washington Seattle Campus, Chemical Engineering Beck, David; University of Washington, Chemical Engineering; University of Washington, eScience Institute Pozzo, Lilo; University of Washington, Chemical Engineering; University of Washington, Materials Science & Engineering

SCHOLARONE™
Manuscripts

ARTICLE

High-Throughput and Data Driven Strategies for the Design of Deep-Eutectic Solvent Electrolytes

Jaime Rodriguez Jr.^{a†}, Maria Politi^{a†}, Stuart Adler^a, David Beck^{a,b}, and Lilo Pozzo^{a,c,†}

Received 00th January 20xx,
Accepted 00th January 20xx

DOI: 10.1039/x0xx00000x

Deep eutectic solvents (DES) are an attractive class of materials with low toxicity, broad commercial availability, low costs and simple synthesis, which allows for tuning of their properties. We develop and demonstrate the use of high-throughput and data-driven strategies to accelerate the investigation of new DES formulations. A cheminformatics approach is used to outline a design space, which results in 3,477 hydrogen bond donor (HBD) and 185 quaternary ammonium salt (QAS) molecules identified as good candidate components for DES. The synthesis methodology is then adapted to a high-throughput protocol using liquid handling robots for the rapid synthesis of DES combinations. High-throughput electrochemical characterization and melting point detection systems are used to measure key performance metrics. To demonstrate the new workflow, a total of 600 unique samples are prepared and characterized, corresponding to 50 unique DES combinations at 12 HBD/QAS molar ratios. After synthesis, a total of 230 samples are found liquid at room temperature and further characterized. Several DES display conductivities above 1 mS/cm, with a maximum recorded conductivity of 13.7 mS/cm for the combination of Acetylcholine Chloride (20 mol %) and Ethylene Glycol. All liquid DES samples show stable potential windows greater than 3 V. We also demonstrate that these DES are electrochemically limited by viscosity, both in the conductivity and in the limiting processes on their cyclic voltammograms. Comparison with literature reports show good agreement for properties measured in the high-throughput study, which helps to validate the workflow. This work demonstrates new methods to accelerate the collection of key DES metrics, providing data to formulate robust property prediction models and obtaining insight on interactions between molecular components. Data-driven high-throughput experimentation strategies can accelerate DES development for a variety of applications. Moreover, these approaches can also be extended to tackle other materials challenges with large molecular design spaces.

Design, System, Application

Deep eutectic solvents (DES) are considered inexpensive designer solvents for a variety of applications, from separation processes to energy-related systems. Type III DES are formed by combining a quaternary ammonium salt and a hydrogen bonding species (e.g., polyols, carboxylic acids or amines), making their design space extremely large. Unfortunately, there is still a significant lack of available data and properties for only a few DES combinations have been tested experimentally. Herein, a strategy is proposed for outlining and experimentally investigating this class of solvents. Starting from their available literature, a cheminformatic campaign to identify their molecular space was conducted using open-source software and databases. Candidate molecules were first screened for their commercial availability and successively selected through a ranking system based on key engineering metrics. Their traditional synthesis route was then translated into a high-throughput protocol making use of liquid handling robots and well-plates. Electrochemical properties and onset of melting were then identified using screen-printed electrodes and an open-hardware IR bolometry system, respectively. Finally, all the data collected was analyzed using open-source packages and Python-based code, made available in its entirety. The methods outlined in this study can be easily applied to other materials design problems with large design spaces.

Introduction

Deep eutectic solvents (DES) are composed of two or more materials that, when mixed at specific molar ratios, exhibit much greater suppression of the melting point than one would

predict assuming an ideal liquid solution.¹ Abbott et al. identified several types of DES, including many that are formed by mixing a quaternary ammonium halide salt (QAS) and a molecular hydrogen bond donor (HBD) at specific molar ratios.² DES have also been frequently compared to ionic liquids (IL), because they have similar notable qualities including, low vapor pressure, low flammability, and an expansive chemical design space allowing for tuning properties.^{3,4} In recent years, both DES and ILs have been proposed as potential electrolytes for electrochemical applications, including redox-flow batteries (RFBs) which are a promising grid-scale energy storage technology.^{5–9} DES and ILs have good ionic conductivities and a wide stable electrochemical potential window compared to

^a Department of Chemical Engineering, University of Washington, Seattle, USA.

^b eScience Institute, University of Washington, Seattle, USA

^c Department of Materials Science & Engineering, University of Washington, Seattle, USA

[†] These authors have contributed equally to this work.

[‡] Corresponding Author

Electronic Supplementary Information (ESI) available. See

DOI: 10.1039/x0xx00000x

aqueous electrolytes.^{10,11} A strong emphasis has also been placed on RFB materials that are low-cost and environmentally friendly.^{12–14} In this regard, DES have an advantage over ILs because they are generally composed of inexpensive and widely available materials that are frequently biodegradable and non-hazardous.¹⁵ Additionally, the synthesis of DES is straightforward and inexpensive, which usually consists of mixing solid components at specific molar ratios and heating until they melt. Moreover, recent studies using DES as electrolytes in RFBs have reported increased solubility of redox species, particularly redox-active organic molecules (ROMs), which subsequently lead to increases in energy density.^{16,17} For these reasons, the use of DES as electrolytes for RFBs is very attractive.

However, major challenges exist for the molecular design of ideal DES electrolytes. The literature states that the total number of possible DES candidates likely exceeds the estimated design space for ILs (estimated at $\sim 10^{18}$ unique anion/cation pairs).^{18,19} Yet despite the simple synthesis process for DES, current experimental efforts and methods have been slow to make a significant dent in exploring these materials. Thus, computational methods have become a powerful tool to provide insight where experiments may fall short. Unfortunately, a common theme amongst computational studies on DES is the lack of data available to make significant

strides in developing generalized predictive models. Moreover, there is a lack of chemical diversity in the available experimental literature since many reported DES systems are overwhelmingly based on choline chloride, a commonly used QAS.^{20–22} Deeper fundamental understanding of DES is also necessary, especially when determining their feasibility for use as electrolytes.²³ The strong hydrogen bond network that is formed in DES has direct impacts on several key electrolyte properties, which can be influenced by molecular weight, QAS anions, and the presence of specific functional groups. Still, many of the features that can lead to ideal DES electrolytes may not be intuitive to determine, and therefore the development of this class of materials will require optimization, functional design, and new methods to tackle exploration of the large design space.

High-throughput experimentation and data-driven strategies for chemical exploration promises to accelerate the development of new materials, including new electrolytes.^{24–27} However, to our knowledge these methods have not yet been applied towards development of DES electrolytes. The design of new materials is known to be inherently a multivariate task requiring solutions aiming at the simultaneous optimization of several target properties. Multi-objective optimization (MOOP) strategies have become increasingly popular, especially in the drug discovery field.^{28–30} However, these techniques rely on available predictive frameworks, databases or molecular

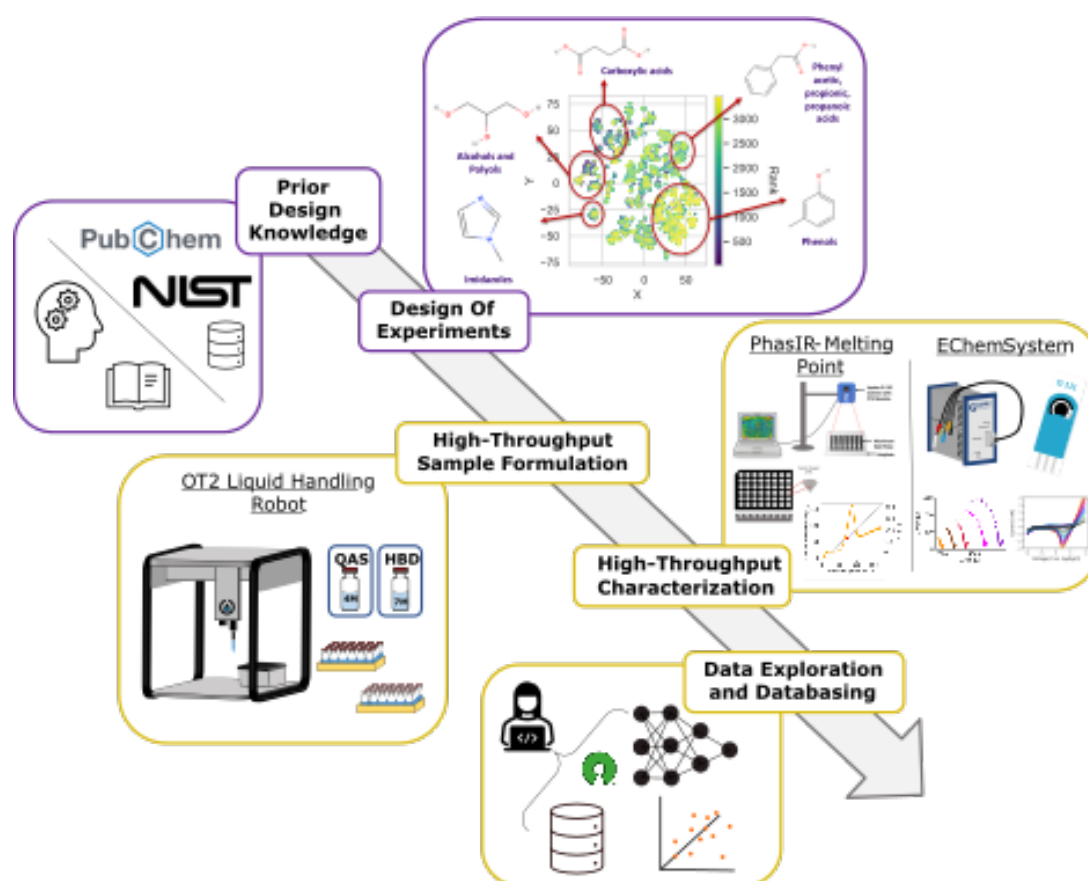


Figure 1 Schema for the high-throughput protocol for DES selection, processing, and characterization. The purple boxes represent the initial data-driven candidate selection for both DES components (QASs & HBDs), whereas the gold boxes represent the automatic sample formulation, processing, characterization, and final data analysis of the prepared samples.

simulations providing a variety of measured or estimated properties for the chemicals used. Unfortunately, the lack of variety of tested combinations and sparsity in their measured properties in the DES literature hinders the formulation of robust models. Furthermore, MOOP systems need to be coupled with medium or high-throughput strategies to best achieve the desired outcome of faster identification of materials with desired properties. Without these experimental infrastructures, the bottleneck of the task would simply shift onto the synthesis and testing phase. In this work we present an integrated workflow for the investigation of DES electrolytes for future use in RFBs. A preliminary cheminformatics approach focused on specific engineering metrics (e.g., chemical similarity, commercial availability) is presented to outline the design space for DES materials and to strategically select initial candidates for exploration using a ranking system which considers scores based on the materials hazards score and their molecular weight. The synthesis process for DES has been modified to enable high-throughput sample preparation using open-source, automated liquid handling robots. Electrochemical characterization is then performed in a high-throughput manner using screen-printed electrodes (SPE) which require minimal sample volume and facilitates data collection and analysis. We have demonstrated that this significantly speeds up sample preparation for large number of samples and allows for a systematic, combinatorial sequence to explore DES.

Experimental

Materials

Acetylcholine Chloride (AcChCl) ($\geq 99\%$), Tetraethylammonium Chloride (TEAC) ($\geq 98\%$), Tetrapropylammonium Bromide (TPAB) (98%), and Tetraethylammonium Iodide (TEAI) (98%) were obtained from Sigma Aldrich (Burlington, MA). Choline Chloride (ChCl) (99%) was obtained from Acros Organics (Fair Lawn, NJ). All QAS were dried under vacuum for 24hr upon receipt and were then stored inside an airtight desiccator to prevent significant water uptake.

Ethylene Glycol (Certified) was purchased from Fisher Scientific (Hampton, NH). Glycerol ($\geq 99\%$), Acetamide ($\sim 99\%$), N, N'-dimethylurea ($\geq 99\%$), 3-phenylpropionic Acid (99%), L-serine ($\geq 99\%$), 4-Amino-4H-1,2,4-triazole (99%), and Xylitol ($\geq 99\%$) were purchased from Millipore Sigma (Burlington, MA). Phenylacetic Acid (99%) was purchased from Alfa Aesar (Haverhill, MA). Urea (Ultrapure) was purchased from Thermo Scientific (Hampton, NH). Ethanol (100 Proof) was purchased from Decon Laboratories (Montgomery County, PA). All HBD were used as received and required no further processing.

High-Throughput DES Synthesis

The high-throughput synthesis process begins with the preparation of concentrated stock solutions of QAS and HBD in volatile solvent, with either water or ethanol being utilized depending on which yielded the greatest solubility for the starting material. See Table S1 and S2 for more information of

final concentrations and solvent used for each stock prepared. The Opentrons OT-2 liquid handling robot was used to prepare the mixtures of QAS and HBD. The concentrations of the stock solutions, along with the desired molar ratio of QAS and HBD mixtures are fed into a python script that first calculates the correct volumes of stock solution to dispense to achieve the

desired DES composition using the system of equations below:

$$V_{QAS} + V_{HBD} \cong V_{Total} \quad (1)$$

$$\frac{C_{QAS} \cdot V_{QAS}}{(C_{QAS} \cdot V_{QAS} + C_{HBD} \cdot V_{HBD})} = X_{QAS} \quad (2)$$

$$\frac{C_{HBD} \cdot V_{HBD}}{(C_{QAS} \cdot V_{QAS} + C_{HBD} \cdot V_{HBD})} = X_{HBD} \quad (3)$$

Although the volumes of solutions are not additive, this approximate equation is still useful to estimate the maximum volumes that can be delivered to avoid overflowing sample containers, to produce enough DES material for testing, and to estimate the minimum volume of stock solutions to complete an experimental campaign. Equations (2) and (3) are analogous to expressions for the mole fraction of a two-component mixture, where C_{QAS} and C_{HBD} are the molar concentration of the QAS and HBD stock solutions, and X_{QAS} and X_{HBD} are the mole fractions of QAS and HBD to produce the selected DES composition. Knowing the total desired volume of mixture, concentration of stock solutions, and molar composition of the DES to synthesize, this becomes a system with 3 equations and 2 unknowns which can be solved trivially. Once the volumes of stock solutions to dispense are calculated by this script (see supplementary files), they are then saved as a '.csv' and passed on to protocol scripts which contains hardware specifications and commands for the OT-2 to perform. The OT-2 liquid handling robot has 11 customizable slots to hold a variety of hardware, including pipette tips, stock solutions, and vials. Samples can be prepared in a variety of standard multi-well plate formats. In addition to these, custom 48-well plates were designed using a 3-D resin printer (FormLabs Form 3) with a temperature-resistant resin that is stable up to 238°C. These plates hold 2 mL glass scintillation vials in each well. The OT-2 is then programmed to directly dispense the correct combination of stock solutions into each of the vials. All files required to reproduce the custom labware described in this paper can be found in a GitHub repository.³¹

After the samples are prepared, it is necessary to remove the volatile carrier solvent so that only the QAS and HBD remain. This is done via a series of gentle evaporation and heating steps. Once the mixtures are created in the OT-2, all 48-well plates are moved to a large commercial dehydrator (Cabela's 80L SKU: 2517102) for a gentle evaporation step at 65°C for at least 24 hours. This initial step removes most of the carrier solvent. Samples are then heated in an oven at 100°C for 30 min, which ensures the formation of a homogeneous mixture, as reports have indicated that heating below 80°C may sometimes result in the formation of precipitates or crystals

upon cooling.^{32,33} Preparing the DES in glass vials allows us to incorporate important aspects of their synthesis (i.e. heating to 100°C or higher), while also aiding in preserving and storing samples for characterization later in the pipeline. Finally, samples are allowed to cool and are dried under vacuum at room temperature for 30 min, to remove any potential residual carrier solvent that could remain, and afterwards stored in airtight desiccators until screening and characterization is performed. Figure 2 shows a schematic of the high-throughput synthesis workflow

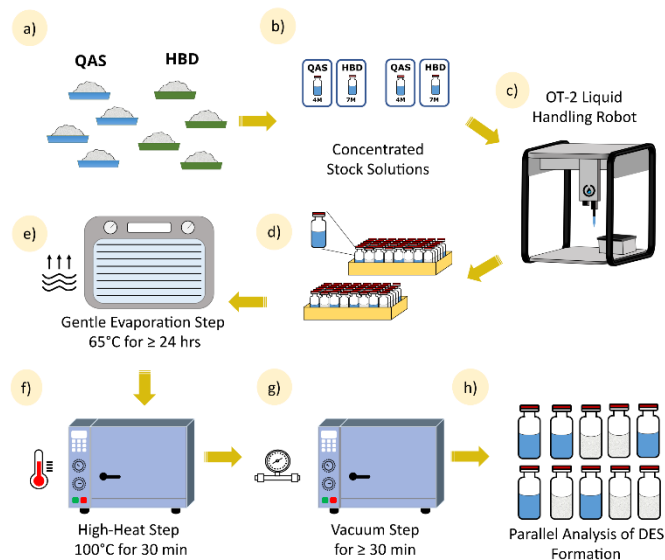


Figure 2 Schematic illustration of the proposed high-throughput synthesis protocol for deep eutectic solvents. a) Each component is weighed and dissolved in either water or ethanol to create highly concentrated stock solutions. b) The stocks, labware, and pipette tipracks are loaded onto the OT-2 deck and the sample formulation is initiated. c) The DES samples and solvents are organized in temperature-stable 48-well plates holding glass vials. d) The sample plates are placed in a dehydrator at 65 °C for 24hrs. This step removes most of the volatile solvents used to transfer the DES components. e) The sample plates are then placed in an oven at 100 °C for 30 minutes. f) The sample plates then moved into a vacuum for about 30 minutes. g) The samples found in the liquid phase at room temperature are now ready to be characterized.

High-throughput Melting Point Determination

The melting point of the samples was measured using a recently developed high-throughput and open-source thermal analysis system called PhasIR.³⁴ This method uses IR bolometry to analyze phase transitions in liquids in a parallel analysis platform. The system consists of a Raspberry Pi microcomputer, a FLIR LEPTON 3.5 IR camera, and aluminum multi-well plates as the basic elements, Figure S5. Its functionality is very similar to differential thermal analysis (DTA). In the PhasIR system however, instead of the thermocouples used in DTA, the temperature of the plate and sample are measured using an IR camera during heating, and the onset of melting is determined by the ΔT curve between the reference (plate) and the sample temperatures. For any binary mixture near a eutectic composition, we expect the solid to liquify over a range of temperatures, starting at the eutectic temperature. Thus, the onset of melting is a good metric for the lowest liquid temperature one can achieve using the chosen mixture, even

when the eutectic composition is not known precisely. The DES samples were cooled using the Peltier plate of the PhasIR hardware system, while the heating process was conducted using a VWR hot/stir plate (NA CAT No: 97042-682) to achieve a broader temperature range. To extract accurate melting temperatures, the PhasIR system and hotplate were moved into a glovebox to conduct the measurement in a moisture-free environment. This step was found to be critically important since many DES tend to be hygroscopic. The samples were loaded on metal 48 or 24 conical-shaped-wells plates, cooled for approximately 2 hrs using the Peltier plate set at -10°C . The hotplate was previously set to 200°C and the measurement took approximately 10 minutes per plate to collect. The data was then analyzed using the homonymous Python-based software which can be found on GitHub.³⁵

High-Throughput Electrochemical Characterization

All electrochemical characterization was performed on a Gamry Reference 600 potentiostat with Metrohm-DropSens DRP-11L SPEs, which were interfaced directly with the Gamry via the Metrohm-DropSens CAC4MMH connector. The DRP-11L is a low cost and disposable compact 3-electrode screen printed cell, making it ideal for working with sample volumes of approximately $100\ \mu\text{L}$. The cell consists of carbon working and counter electrodes and a silver/silver chloride reference electrode. Measurements were conducted only for samples that were liquid at room temperature.

Electrochemical Potential Window Multi-step chronopotentiometry was performed to determine the limiting reduction and oxidation potentials of the DES electrolytes. The use of chronopotentiometry to obtain these potentials has been proposed and reported previously for liquid electrolytes as fast and accurate estimates for comparisons, which facilitates data collection and analysis in the high-throughput pipeline.³⁶ First, a series of four fixed positive currents of 1, 0.75, 0.5, and 0.25 mA are applied. These are then followed by negative currents of the same magnitude. The very first positive and negative steps are held longer, for 15 seconds, as a conditioning step, while each subsequent step is held for 10 seconds with data collected every half second. The voltage response from the current steps will equilibrate towards the end of the measurement, and the potential from the last two seconds of every current step is averaged and extracted for analysis. Tangent lines of the current steps and potentials are calculated from plots of current density vs. potential in both the positive and negative regions and are extrapolated to the line of zero current. The potentials at the line of zero current are the estimated limiting reduction and oxidation potentials for the DES electrolyte. Figures S2 and S3 show example chronopotentiometry data and their analysis using the procedures described above.

Cyclic voltammetry was performed to investigate the possibility of undesired electrochemical side reactions in regions between the limiting reduction and oxidation potentials of the DES electrolytes. Measurements were performed at $100\ \text{mV/s}$ scan rate, spanning voltages from $-2\ \text{V}$ to $2\ \text{V}$, for a

total of four complete cycles per sample to ensure equilibration. Moreover, the last 20 points of the forward and reverse scans were used to determine the slope (dI/dV) of the limiting processes shown in the voltammogram.

Ionic Conductivity Electrochemical Impedance Spectroscopy (EIS) was used to determine the ionic conductivity of the DES electrolytes. EIS is a non-destructive technique that allows for the separation of specific contributions to cell resistance via timescale based on the response of the cell to a sinusoidal voltage or current perturbation. At the highest frequencies probed, electrode current becomes almost entirely capacitive, such that the measured cell impedance (Z) becomes ohmic, with resistance inversely proportional to the ionic conductivity of the solvent. Thus, EIS can be used to isolate ionic conductivity in a system with unknown or variable electrode characteristics. A small voltage perturbation of amplitude 50 mV was applied to the samples and the frequency was varied from 100 kHz to 100 Hz, with a total of 10 points per decade. Once the measurement is completed, the data is visualized using a Nyquist plot in which the negative imaginary component ($-Z_{im}$) of the impedance is plotted against the real component (Z_{re}). The point at which the impedance curve intersects the axis of the real component is extracted as the ohmic resistance of the system. The impedance data was fit using the open source package Impedance.py.³⁷ Due to the unusual geometry of the screen-printed electrochemical cell, a calibration curve was obtained using standards of known conductivity spanning four orders of magnitude (Figure S4) to convert the resistance to a quantitative conductivity. The conductivity standards were: 84 $\mu\text{S}/\text{cm}$, 443 $\mu\text{S}/\text{cm}$, 1413 $\mu\text{S}/\text{cm}$, 2764 $\mu\text{S}/\text{cm}$, and 12880 $\mu\text{S}/\text{cm}$. These were obtained from Oakton (Vernon Hills, IL) and are all NaCl based solutions.

Results and Discussion

Cheminformatic Outlining of the Design Space

In many situations where the design space for a materials problem is very large and prior knowledge about the materials is limited, approaches to outlining the design space can provide insight for developing an effective design of experiment (DOE).^{38,39} With regards to DES, possible candidates for HBD consist of large families of molecules such as alcohols, polyols, amides, carboxylic acids, etc., and in addition many different QAS exist with varying alkyl chain lengths and anion species. Despite the rich materials space for DES, the diversity of candidates studied in the literature is rather low. One of the goals of this work was to outline the commercially available design space for DES materials via a cheminformatics campaign, prior to performing any experimental procedures. This would allow for the rational formulation of a set of promising candidates (basis set) to investigate experimentally without requiring synthesis of precursor materials. As an initial strategy for the basis set selection, the use of engineering metrics and design constraints to filter and rank materials was applied, which aids in assuring promising candidates are identified for

experimental analysis over candidates that lack in one or more engineering metric. The ability to effectively outline a material design space is essential to DOE planning, and while our investigation is focused on DES, we present this approach as a strategy that can be easily applied to other materials problems.

The first step in this process was to procure a basis set of known QAS and HBD that have been previously used in the literature to form DES. The National Institute of Standards and Technology (NIST) is an excellent resource for publicly available material databases, and their ILThermo database contains extensive data for DES.⁴⁰ In total over 2,000 datapoints were obtained for several physiochemical properties across a variety of DES. In addition to ILThermo, a DES melting point dataset was obtained from a review.⁴¹ The datasets were all compiled, and 36 unique QAS and 75 unique HBD were identified.

A starting point from which to identify promising, but perhaps non-intuitive, QAS and HBD candidates that have not been described in the literature was now possible. The concept was to perform an iterative structural similarity search across each of the QAS and HBD in the basis set. This required a platform capable of efficiently applying cheminformatics methods and subsequently querying a large chemical database. For this, PubChem's open-source Python wrapper (PubChemPy) coupled with the Power User Gateway Representational State Transfer (PUG-REST) was chosen due to its relative simplicity and ability to access PubChem's data and services. PubChemPy allows for Python-based interaction to retrieve chemical identifiers, physiochemical property data, and perform

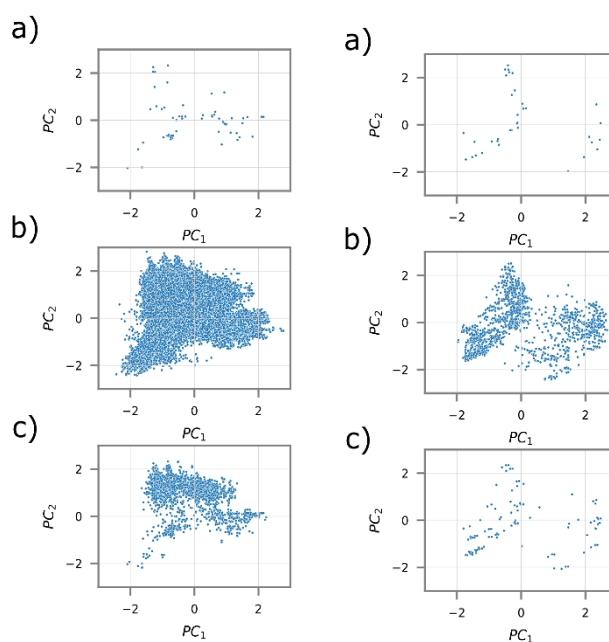


Figure 3 Cheminformatics campaign for HBD species. a) Initial HBD candidates used in published DES work. b) Growth of candidates obtained from the similarity search based on the Tanimoto Scoring Index. c) Final HBD candidates meeting commercial availability and low environmental and human hazards constraints

Figure 4 Cheminformatics campaign for QAS species. a) Initial QAS candidates used in published DES work. b) Growth of candidates obtained from the similarity search based on the Tanimoto Scoring Index. c) Final QAS candidates meeting commercial availability and low environmental and human hazards constraints

chemical similarity searches, among other uses.⁴² PUG-REST can also be used via URL to retrieve data of interest that is not readily accessible by PubChemPy.^{43,44} Compound id's (CID), which are PubChem's unique identifiers, were obtained for the basis set. From these CID's, virtually any information available in PubChem's database can be queried. SMILES strings, which are common linear notations to describe chemical structures, were used to initiate a 2D structural similarity search for each material in the basis set. The PubChem similarity search begins by converting the SMILES strings to molecular fingerprints, which represent chemical structures using binary vectors.⁴⁵ Here, each vector position represents a chemical substructure or feature, whose absence or presence is denoted with a 0 or 1, respectively. While several variations of molecular fingerprints exist, PubChem uses a binary vector of length 881, with predetermined substructures in each vector position.⁴⁶ After the fingerprints are obtained, they are then compared to the fingerprints of all other compounds available in the PubChem database and their similarity is judged by the Tanimoto scoring index.⁴⁷ The Tanimoto index considers the proportion of substructures or features that are shared between two compounds to give a score of similarity. A threshold can be specified in the PUG-REST API for the similarity search to only return compounds that are above a specific similarity score. In our search, a similarity threshold of 85% was used to ensure a balance between results that are adequately similar from the initial compound, but still yield some diversity. In addition, the search was specified to return a maximum of 3,000 results per search to avoid timing out the request on PubChem's servers.

This search resulted in an expanded set of 68,127 and 4,705 complimentary HBD and QAS candidates, respectively, that were returned from the initial NIST basis set (i.e., 75 HBD and 36 QAS). After significantly growing the design space, it was necessary to constrain it again according to metrics that are important to our specific application. For example, only candidates that are readily and commercially available for procurement were to be considered, to avoid the need for costly organic synthesis and purification. In this regard, vendor information was extracted from the PubChem database and scripts were developed to filter candidates that were not commercially available. The code is available in the Supplementary Material. The ability to characterize the environmental and human health hazards of the candidates is another metric deemed important for this work, and therefore safety information from the Globally Harmonized System of Classification and Labelling of Chemicals (GHS) was also extracted. DES precursors that had no GHS safety information available in the database were filtered and removed. Figures 3 and 4 show the subsequent growth and constraint of the design spaces for the QAS and HBD. The visualization was created by representing each of the candidates using Morgan fingerprints. Unlike the PubChem fingerprints used for the similarity search, each bit in the vector for Morgan fingerprints is not constrained to a predefined structure, but instead uses a complex algorithm to generate the bit vector.⁴⁸ The length of the vector can also be specified, and 2,048 bits was selected to obtain more structural information on the candidates. To project this high

dimensional information on a two-dimensional space, Principal Component Analysis (PCA) was used, which is a dimensionality reduction technique for visualization.^{49,50} The final basis set after applying constraints resulted in 3,477 HBD and 185 QAS.

With the final design space defined, a ranking system based on engineering metrics important to our target application was developed to highlight candidates with favorable properties and characteristics. Initially, the ranking system was based two components: the GHS safety hazards codes (i.e., health, environmental, physical) and the molecular weight of each molecule identified in the cheminformatic campaign. The GHS safety scores were developed based on previous examples in the literature, with regards to the specific hazard codes and the

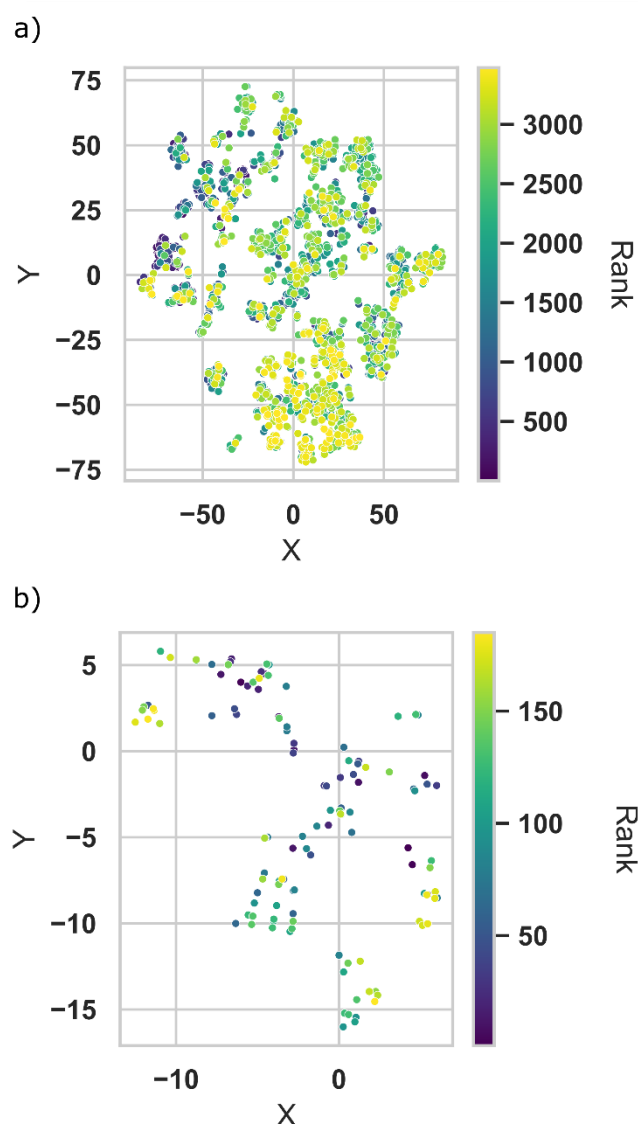


Figure 5 Final design space for HBD (a) and QAS (b) based on 50 principal components in the PCA applied to the original dataset of Morgan fingerprints and reduced to a two-dimensional plot using the non-linear dimensionality reduction technique called t-distributed stochastic neighbor embedding (t-SNE). The color of each candidate is based on its ranking, which considers scores based on GHS safety hazards and molecular weight

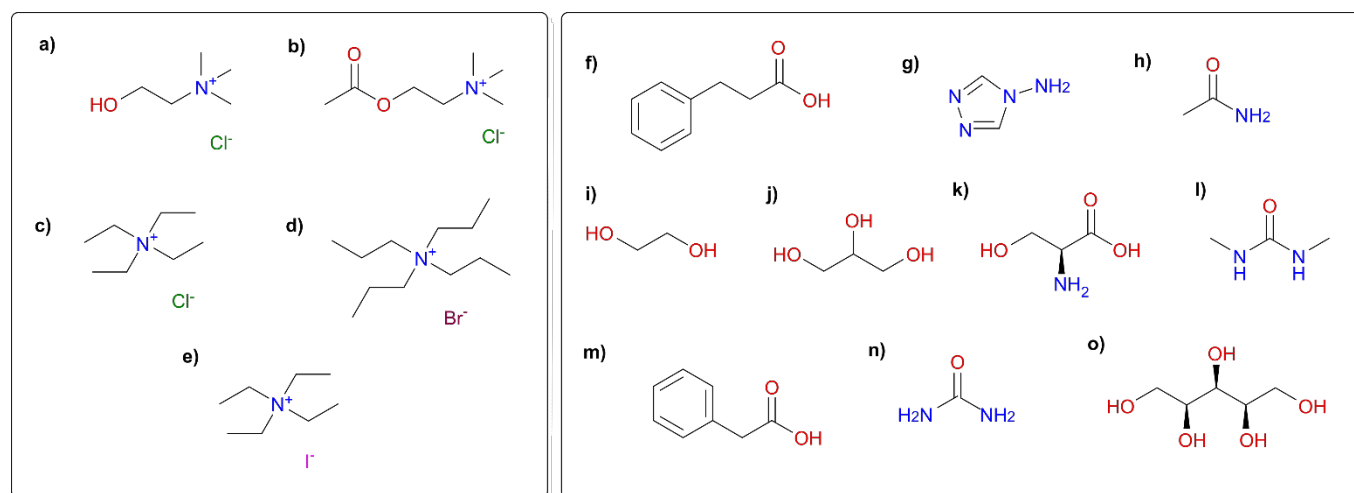


Figure 6 Structures of Quaternary Ammonium Salts (Left) and Hydrogen Bond Donors (Right) selected for high-throughput DES synthesis. The depicted molecules are the following: a) Choline Chloride, b) Acetylcholine Chloride, c) Tetraethylammonium Chloride, d) Tetrapropylammonium Bromide, e) Tetraethylammonium Iodide, f) 3-Phenylpropionic acid, g) 4-Amino-4H-1,2,4-triazole, h) Acetamide, i) Ethylene Glycol, j) Glycerol, k) L-serine, l) N,N'-Dimethylurea, m) Phenylacetic acid, n) Urea, o) Xylitol

severity of the hazard they represented.⁵¹ As for the molecular weight, QAS and HBD with lower molecular weights will generally possess lower melting points as a DES, and so this was a favored characteristic. Next, the molecular weights and the GHS safety scores were all normalized, and a modified digital logic method was utilized to assign a pre-factor to each of the metrics, which determines the weight (i.e., importance) that each metric contributes towards the rankings. The pre-factor is assigned based on the comparative importance of each of the metrics with each other. For example, health hazards were regarded as the most important parameter compared to the molecular weight and was therefore assigned the highest pre-factor. This digital logic method has been commonly used for ranking engineering metrics for a wide variety of material sections.⁵² In future queries, other metrics (e.g. cost, sustainability) could also be easily incorporated into this ranking approach for additional DOE campaigns.

With each of the candidates now ranked in the design space, it is possible to visualize the ranked molecular space. However, we see in previous visualizations that while the size of the molecular space is apparent, clusters or groupings of candidates by molecular structures are not. This is because the PCA only utilized the two most important principal components for plotting, resulting in loss of structural information contained in the Morgan fingerprints. To recover that information, it is necessary to increase variance by increasing the number of principal components. However, that creates a challenge for visualizing high-dimensional spaces. To solve this problem, a non-linear dimensionality reduction technique called t-distributed stochastic neighbor embedding (t-SNE) is used.^{53,54} The number of principal components in the PCA, that was applied to the original dataset of Morgan fingerprints, was increased to 50 and reduced to a two-dimensional plot with t-SNE. Figure 5 shows the resulting t-SNE plots with the HBD and QAS. As for the HBD, clearly distinct clusters of molecules with similar structure are observed. The clusters in the QAS are not

as clear given the smaller number of molecules in that dataset, yet some distinctions can be made. In addition to these plots, an accompanying python script was written to interactively visualize the space and directly select areas to view the molecules' structure and their corresponding ranking. It is now possible to use this information to rationally select candidate HBD and QAS chemicals for our initial DOE campaign, to maximize chemical diversity and information content while also increasing the likelihood that an experimentally analyzed DES is more likely to be viable for practical implementation.

High-throughput DES synthesis

An advantage of DES is that their synthesis is relatively straightforward, simple, and cost effective. Samples are prepared in the traditional method by adding the pure QAS and HBD components together in vials at the appropriate molar ratio, followed by heating and stirring until they result in a uniform liquid. While some of these components are liquid in their pure form (i.e., ethylene glycol, glycerol, trifluoroacetic acid) the majority are usually solids. While the approach is suitable for investigating a small quantity of DES at a time, it quickly becomes inefficient when attempting to explore a broad range of potential DES across various molar ratios. Instead, we have developed a low-cost (< \$10k) workflow to synthesize DES in high-throughput, where sample volumes of typically less than 2 mL are prepared, leading to lower consumption of raw materials but an increase in the diversity of samples investigated. Since the OT-2 pipetting robot has limited space for sample labware, stock reservoirs, pipette racks, the samples will be formulated in different runs. In fact, using the custom designed 48-well plates, we were able to prepare up to 240 samples (i.e., five 48-well plates or all combinations of the 10 HBD with 2 QAS) per run. The OT-2 protocol includes mixing steps, to minimize the formation of two distinct phases and aid in the interaction of the DES components, as well as steps to reduce the possibility of sample contamination and satellite

droplet formation. See Figure S1 for an example OT-2 deck configuration and the supplemental Jupyter Notebook for example scripts. To demonstrate these methods, a variety of DES based on 5 QAS and 10 HBD were prepared, Figure 6. This selection included some QAS and HBD that are common in the literature, which we use for validation of the workflow, in addition to others that were selected from the outlined DOE design space (Figure 5). This gives a possible combination of 40 new DES that could be prepared. It is important to note that, while a few of these materials have been presented in the literature (e.g., choline chloride, acetylcholine chloride, urea, ethylene glycol, and glycerol, among others), the total combinatorial space has not been investigated to the fullest potential. For example, nearly all HBD selected in this set have been paired with ChCl to form DES.^{55–59} Here, we have broadened the investigation to additional QAS, with ChCl based samples prepared as a comparison with literature. Therefore, prior to even delving into the expanded design space, there is an abundant combinatorial space that needs to be investigated just from materials that have already been reported. The high-throughput system proposed is suited to tackle that challenge.

Each of the selected HBD and QAS were dissolved in concentrated stock solutions in either water or ethanol (See Table S1 and S2), and the OT2 protocol prepared 12 molar compositions (Table S3) for each of the 40 DES combinations and the additional 10 ChCl-based combinations. In total, this yielded 600 samples that were prepared in our high-throughput method. After samples were processed through the evaporation, heating, and vacuum steps, it was noted that samples containing ChCl, AcChCl, TEAC, and TPAB as QAS formed liquids at room temperature. All liquid samples were clear and showed a homogeneous phase. In contrast, all samples containing TEAI as a QAS did not form a liquid at room temperature with any HBD combination and therefore were not characterized further. Similarly, all the samples that used L-serine as the HBD species were found solid at room temperature. So, these were also excluded from electrochemical testing.

High-throughput Characterization of Melting

The melting point of the synthesized the choline chloride-based samples was characterized using the PhasIR system, which is thoroughly described in a recent publication.³⁴ An example plot can be seen in Figure 7, right. Here, the temperatures of samples and the aluminum plate are encoded in the pixel value composing the frames collected by the Lepton IR camera. The sample temperature is obtained from the average pixel values across a circular region of that is positioned around the centroid of each well across all frames of the video. For each well identified on the image, the plate temperature is averaged over four equidistantly points placed diagonally with respect to the well centroid. An example image of the metal 48-well plate with centroid and plate position identification obtained through the PhasIR *Image Analysis* module can be found in Figure 7, left. Samples and plates are then heated from a low temperature and the temperature of the sample (T_{sample})

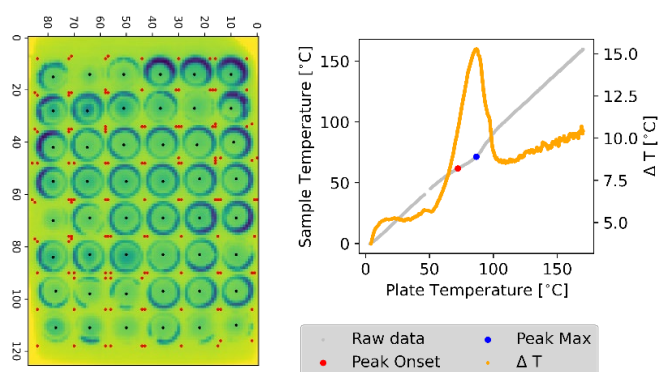


Figure 7 Left) Example 48-well well plate with centroid and plate temperature identification obtained through the PhasIR *Image Analysis* module. The black marker identifies the centroid of the well, whereas the red marked are used as the reference plate temperature for each well. Right) Melting point for the 35 mol%: 65 mol % choline chloride: N,N-dimethylurea sample. The temperature was recorded using the PhasIR system. The melting point is defined as the onset (red marker) of the $\Delta T = T_{plate} - T_{sample}$ curve (yellow)

is plotted with respect to the temperature of the plate (T_{plate}). For most of the heating process, there is a linear relationship between the two temperatures. However, when samples melt, there is a discontinuity in this plot due to the abrupt change in the thermal conductivity of the sample. Thus, for each sample in the plate, the onset of the phase transition event is obtained from the onset of the peak formed by the $\Delta T = T_{plate} - T_{sample}$ curve. The peak onset is determined using the Scipy peak finding algorithm.⁶⁰ The PhasIR measurements were conducted in an argon-filled glovebox to reduce the possible contamination with atmospheric water during the sample's physical characterization. Still, a small portion of measured samples show a phase transition feature close to 0 °C, which could be attributed to traces of water in the samples. For example, Figure S16a shows PhasIR measurements for the 60 mol% ChCl sample with acetamide. This is the only case in which the feature is so noticeable, in other cases, the 'water feature' is only a small shoulder in the ΔT curve in the lower temperature region of the measurement (Figure S16b). If samples do not show a clear phase transition feature (Figure S17), they are not included in the final phase diagrams, since this likely means that the phase transition temperature is outside of the measurement range of the PhasIR system. In the literature, the freezing temperature of DES solvents is commonly reported using differential scanning calorimetry (DSC) in the cooling cycle. However, DSC is a low-throughput technique that takes over 60 minutes per sample, and it is not suitable for the exploration of large design spaces of DES system. In contrast, the infrared bolometry technique that is used in the PhasIR system is well suited for fast screening of up to 96 samples simultaneously in ~10 minutes. On the other hand, it is unfortunately very hard to identify phase transitions in the PhasIR system during cooling cycles (freezing) due to the very slow cooling rates of Peltier plates and the variable nucleation rates of different DES samples. Therefore, reported phase transitions in this work correspond to the 'first onset of melting' for the samples tested, which may not always

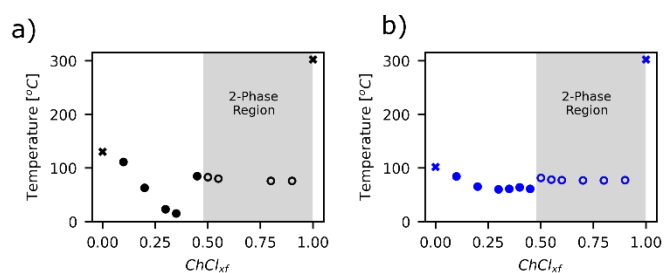


Figure 8 Phase diagrams for urea (a) and N,N'-dimethylurea (b). The filled circular markers indicate measurements obtained using the PhasIR system. The x-shaped markers indicate literature values for the pure components.

correspond to the complete homogeneous melting of DES samples. In fact, for samples containing high ratios of QAS, this phase-transition point often indicates partial melting of a solid sample to a two-phase sample containing a liquid and a dispersed solid. This is clearly outlined by a gray area in the results. Figure 8a Figure 8b shows PhasIR melting-onset diagrams for the urea and N,N'-dimethylurea samples, respectively. The eutectic point for the ChCl: urea samples was clearly identified at the expected 1:2 molar ratio, which is consistent with literature reports.⁶¹ The onset-melting diagrams for the two phenyl carboxylic acids can be seen in Figure S16 and they both also show a single eutectic temperature depression around the 35 mol% of choline chloride sample, again in line with samples synthesized using the traditional methodology.⁵⁹

On the other hand, the diagram for N, N'-dimethylurea seems to show a broad low-melting point region followed by a flat two-phase melting region. A broad melting region is also present in the phase diagrams for 4-Amino-4H,1,2,4-triazole and acetamide, Figure S19a, b. Unfortunately, it was not possible to measure transition temperature below 0°C in high-throughput with the PhasIR system. For this reason, the diagram for ethylene glycol and glycerol DES could not be obtained as the melting temperature is much lower than can be reliably measured with PhasIR. For xylitol-based samples with choline chloride, the eutectic point was found at a 1:1 ratio (Figure S20), which is also in agreement with literature.⁶² All of the melting diagrams also show complex melting behavior at higher content of QAS. At values above ~55 mol% of the QAS, there is usually phase separation between a solid QAS dispersion and a mixed QAS/HBD liquid phase (Figure S22).

Table 1 Choline Chloride-based DES Melting point comparison between literature values and those measured in the current publication using the PhasIR system.

Ratio	HBD	Current Publication	Literature Values	Source
		[°C]	[°C]	[–]
1:2	Urea	15	12	⁶¹
1:2	N, N'-Dimethylurea	63.3	70	⁶¹
1:2	Acetamide	27.5	50	⁶¹
1:2	Phenylpropionic Acid	21.6	20	⁵⁹
1:2	Phenylacetic Acid	14.5	25	⁵⁹
1:1	Xylitol	3.6	RT	⁶²

Table 1 shows a comparison of the eutectic temperatures measured using the PhasIR system with those reported in the literature. Agreement is generally excellent, with most measurements within ~5°C. Only the DES samples formed between choline chloride and acetamide and phenylacetic acid, both at a 1:2 ratio (QAS: HBD), show lower values compared to their respective published values. This could again be due to moisture or residual water in the hygroscopic samples, which is known to depress the melting points of DES. Other results obtained for choline chloride samples synthesized using the high-throughput protocol are in great agreement with published values. This supports the use of this high-throughput workflow to investigate the melting temperatures of DES.

High-throughput Electrochemical Characterization of DES

The ability to screen and identify DES electrolytes in a high-throughput manner with high ionic conductivities and wide electrochemical potential windows is crucial to their performance optimization. However, most electrochemical measurements are still conducted with bulky electrodes and relatively large samples (~10 mL is typical) that are not conducive for screening large design spaces. In this work, we use screen printed electrodes (SPE) that require minimal sample volume (~100 µL) and are ideal for conducting measurements of multiple samples in very short periods of time (~7 min/sample for all three electrochemical measurements conducted). These SPEs can be interfaced directly with standard electrochemical equipment, converting them into a high-throughput platform for parallel data collection and batch analysis. The DES synthesized in the high-throughput process were then characterized by this high-throughput electrochemical setup. Once again, only samples that were found to be liquid at room temperature, (19 – 24 °C) were characterized, which consisted of DES with ChCl, AcChCl, TEAC, and TPAB as QAS. We would like to note that the 'liquid at room temperature' constraint for the electrochemical characterization was only enforced in the current workflow due to testing limitations of the high-throughput set up. However, it is anticipated that RFB operation can take place at temperatures that can be significantly higher (~80 °C).

Figure 9 shows the ionic conductivities of the DES electrolytes. Immediately some interesting trends can be noticed. It is abundantly clear that variations in the molar composition in the DES with respect to the QAS and HBD components greatly affects the conductivity, which is because of changes in viscosity and ion concentrations. All DES samples based on ethylene glycol as HBD, regardless of their QAS component, showed the highest conductivities. The sample at 20 mol % AcChCl having the highest conductivity in the entire dataset at approximately 13.7 mS/cm. Compared to published values of ionic conductivities for DES, this seems to be the highest recorded for this class of materials. In fact, the largest reported conductivity we could find was for the (3:7) choline chloride-imidazole DES at 12 mS/cm (333K).⁶³ Conductivities for ethylene glycol-based DES with ChCl, TEAC and TPAB were also relatively large with maximum conductivities of

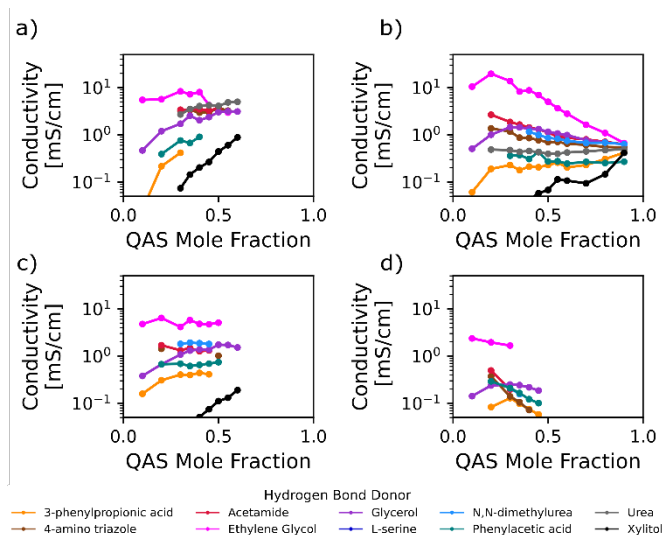


Figure 9 Plots of ionic conductivity of DES electrolytes extracted from potentiostatic electrochemical impedance spectroscopy measurements. The ionic conductivity is associated with the ohmic resistance, shift in the Z_{re} on the Nyquist plot. a) Choline Chloride (ChCl), b) Acetylcholine Chloride (AcChCl), c) Tetraethylammonium Chloride (TEAC), d) Tetrapropylammonium Bromide (TPAB)

approximately 8.3 mS/cm , 6.4 mS/cm and 2.4 mS/cm , respectively. Typically, DESs based on ethylene glycol are known for possessing relatively high conductivities, as the viscosity of ethylene glycol is very low. On the opposite end, DESs based on xylitol possessed the lowest conductivities in the dataset.

DES with sugar based HBD, such as xylitol, are known to have high viscosities, so it is intuitive that conductivities for these DES would be quite low, especially for the xylitol-based DES with $10 \text{ mol } \%$ TPAB which only exhibits a conductivity of approximately 0.001 mS/cm .⁶⁶ Comparing the evolution of the conductivity between the ethylene glycol and xylitol DES, important distinctions can be made. It is seen with all DES containing xylitol that the conductivity begins to substantially increase as the mole fraction of QAS increased. This is intuitive as one would expect that greater concentrations of ionic species would increase conductivity, which has been proposed for all DES.⁶⁷ While ChCl DES samples seem to follow this trend, data collected herein suggests that this is not universal. Notably, we observe for AcChCl based DES with ethylene glycol and glycerol that conductivity decreases significantly with increasing QAS

concentration. This could suggest that increased QAS concentrations result in increased viscosities, which would reduce the conductivity by hindering the mobility of ions in solution. When looking at ethylene glycol- and glycerol-based DES with TEAC, the conductivities either remain relatively constant or increase slightly, and changing the QAS to TPAB causes the conductivities to behave like AcChCl. Moreover, previous studies have noted that the conductivity of DES may evolve through a maximum.⁶⁸ This is noted particularly with ethylene glycol and glycerol based DES, but is also observed in AcChCl and phenylacetic acid, which exhibits a maximum conductivity at $45 \text{ mol } \%$ AcChCl. In general, aside from investigating the conductivities at either extreme, most DES other than those containing ethylene glycol or xylitol, fall within a range slightly above or below 1 mS/cm .

Keeping in mind the proposed use for these solvents, the conductivity of the electrolytes is a crucial metric affecting the performance of a RFB and its operating conditions. Looking at literature studies of the electrochemical properties of DES, there is still a significant gap in data for DES based on QASs that are not ChCl. Therefore, we are not able to directly compare our results to traditional synthesis routes for samples containing AcChCl, TEAC or TPEB as their QAS. Nonetheless, for ChCl-based DES, we notice that our results are in very good agreement with literature values. This confirms that the high-throughput synthesis approach can produce DES materials of similar quality to those reported in the literature (Table 2). For samples containing ChCl and ethylene glycol, phenylacetic acid or phenylpropionic acid as the HBD, our measurements show similar values to published ones.^{59,64,65} On the other hand, the urea- and glycerol-based DES we formulated show elevated conductivities. The increase in conductivity could be due to moisture absorbed from the environment or to residual water from the synthesis process. On the other hand, for the ChCl-urea DES, there are discrepancies among values in literature.^{59,64} In fact, even though reported quantities are measured at slightly different temperatures, there is an order of magnitude difference between these. The values we obtain in this work are closer to those from Shah et al., while still being higher.⁶⁴ Still, there is generally good agreement between conductivities of DES samples produced via our high-throughput workflow and most published results of similar compositions.

Table 2 Conductivity measurements of Choline Chloride-based DES and their comparison with reported literature values.

QAS	HBD	Ratio	Literature Values			Current Publication		
			Temp	Conductivity	Source	Temp	Conductivity	QAS_{xf}
			[°C]	mS/cm	[-]	[°C]	mS/cm	[-]
ChCl	Phenylacetic acid	1:2	25	0.48	59	19-24	0.67	0.35
ChCl	Phenylpropionic acid	1:2	25	0.32	59	19-24	0.42	0.3
ChCl	Urea	1:2	30	2.31	64	19-24	3.5	0.35
ChCl	Urea	1:2	25	0.75	59			
ChCl	Ethylene Glycol	1:2	20	7.61	65	19-24	7.32	0.35
ChCl	Ethylene Glycol	1:2	25	7.33	64			
ChCl	Glycerol	1:2	20	1.05	65	19-24	2.55	0.35
ChCl	Glycerol	1:2	25	1.18	56,59			
ChCl	Glycerol	1:2	25	1.75	64			
AcChCl	Urea	1:2	40	0.017	59	19-24	0.417	0.35

Results of the high-throughput electrochemical measurements of the potential window of the various DES are shown in Figure 10. Current RFBs are typically based on aqueous electrolytes with operating voltage windows of approximately ~1.23 V that are limited due to water electrolysis.⁶⁹ The DES electrolytes tested here show stable potential windows that are at least twice as high as standard aqueous electrolytes (range of 2.5 V to 5 V). While electrochemical studies with large diversity of DES species are scarce, variations in the values of the potential windows for the same species in multiple studies are noted due to the surface activity of the selected electrode material. For example, Li et al. reported variability in the potential window of various ILs on gold, platinum, and glassy carbon working electrodes, noting that the glassy carbon electrode generally possessed the largest potential windows.⁷⁰ Similar trends are noticed in DES by Bahadori et al., where the potential windows of 1:1 ChCl:Oxalic acid and 1:1 ChCl:Malonic acid were measured. The potential windows on GC electrodes for both DES were 2.64 V and 2.1 V, respectively, whereas on a platinum electrode they were 1.62 V and 1.43 V, respectively.⁷¹

Once again, due to the lack of diversity in DES composition published in the literature, we are only able to compare results for samples prepared with choline chloride. Generally, samples in this work have slightly smaller stable electrochemical potential windows (EPW) when compared to those reported by Li et al.⁷² This could again be due to the presence of moisture and/or residual water in DES samples that are very hygroscopic. Nevertheless, the potential windows presented in this study compare reasonably well to those reported in the literature for other DES systems (Table 3). Moreover, RFB systems often use carbon-based electrodes that are like the screen-printed electrodes used in this work. In this study, xylitol- and phenylacetic acid-based DES appeared to show highest variability with respect to molar composition amongst other samples. When paired with AcChCl, xylitol samples have a high potential window of 4.73 V (40 mol % AcChCl) that drops to 3.14 V at higher QAS concentrations (80 mol % AcChCl).

For phenylacetic acid, the trend is opposite as it increases significantly from 2.46 V (30 mol % AcChCl) to 3.04 V (50 mol % AcChCl) and then levels off. Trends are similar when these HBDs are paired with TEAC. It is important to note that certain samples that were shown in the conductivity measurements are not reported in the electrochemical potential window. In fact, certain samples, particularly those with xylitol, were so viscous that the potential required to meet the current at each galvanostatic step was outside the usable range of the

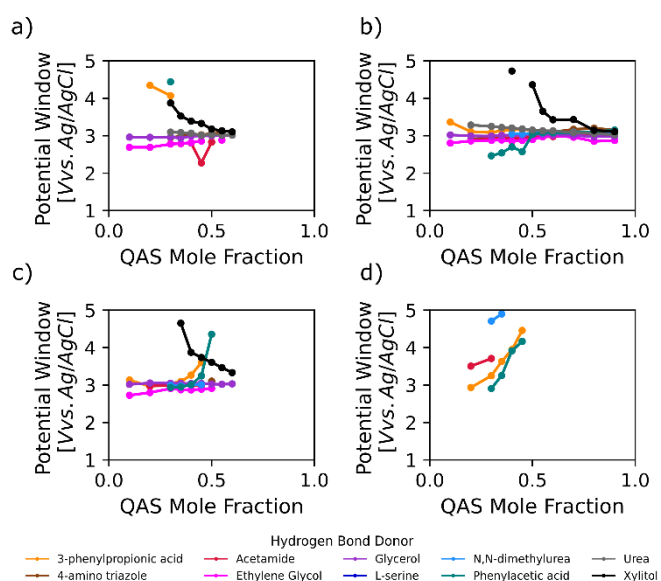


Figure 10 Potential window of DES electrolytes, extracted from chronopotentiometry measurements as a function of the QAS mole fraction. The anodic potential (E_a) is obtained by linearly fitting the average of the last 2 s of each current hold step and extracting the value of the potential at zero current, $E_a = -\frac{\text{intercept}_a}{\text{slope}_a}$. The same procedure is repeated for the cathodic potential (E_c), using the negative current hold steps. The potential window is the difference between E_a and E_c . a) Choline Chloride, b) Acetylcholine Chloride, c) Tetraethylammonium Chloride, d) Tetrapropylammonium Bromide

potentiostat. Furthermore, we noticed that some samples (e.g., 55 mol % ChCl with Ethylene Glycol, TBAB and 4-Amino-1H,1,2,4-Triazole at all the mole ratios) froze during chronopotentiometry. This could indicate that their melting point was very close to the room temperature. Though only a limited number of samples were measured with TPAB, the potential windows was generally above 3V. The highest potential window was 4.9 V for N, N'-Dimethylurea and TPAB at (1:2 mole ratio), which is one of the higher reported in the literature. For most of the samples investigated, the value of the potential window does not vary substantially with increasing QAS concentration. This is expected since the potential window is correlated to the electrochemical degradation of the QAS and HBD.

Inspection of the CVs for the candidate electrolytes reveals insights into the correlation of their electrochemical degradation with respect to the QAS and HBD materials. For example, the CVs of the 3-phenylpropionic and phenylacetic acid HBDs both containing carboxylic acid functional groups are remarkably similar (Figures 11 and 12). In fact, these samples

Table 3 Electrochemical Potential Window (EPW) measurements of Choline Chloride-based DES and their comparison with reported literature values from Li et al.⁷²

QAS	HBD	Ratio	Literature Values			Current Publication				
			E_a	E_c	EPW	Temp	E_a	E_c	EPW	QAS_{xf}
			[V]	[V]	[V]	[°C]	[V]	[V]	[V]	[-]
ChCl	Urea	1:2	1.54	-2.75	4.29	RT	1.23	-1.85	3.08	0.35
ChCl	EG	1:2	1.26	-2.35	3.61	RT	1.13	-1.66	2.79	0.35
ChCl	Glycerol	1:2	1.38	-2.21	3.59	RT	1.15	-1.78	2.99	0.35
ChCl	Xylitol	1:2	1.66	-2.67	4.33	RT	1.29	-2.23	3.52	0.35

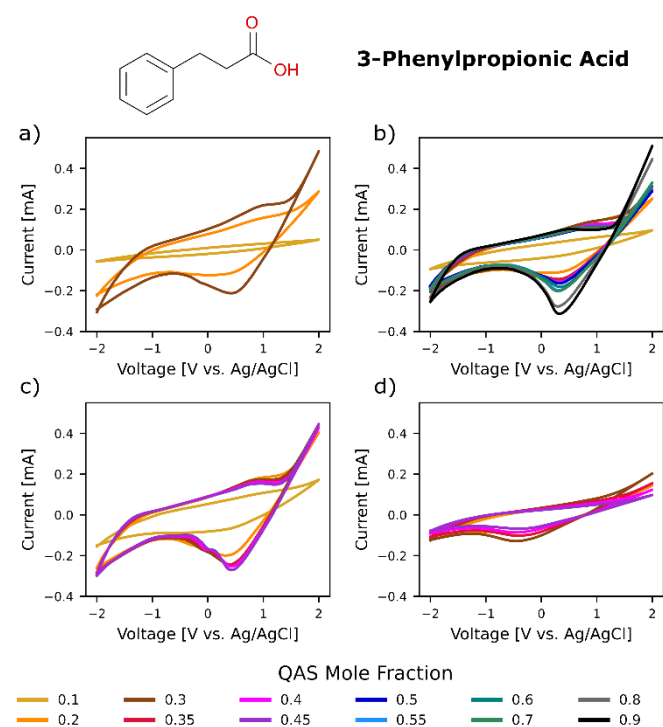


Figure 12 Cyclic voltammograms of 3-phenylpropionic acid-based DES as a function of QAS mole fraction. For all measurement, the potential was varied from $-2V$ and $2V$ with a scan rate of 100 mV/s and a total of 4 cycles per sample to ensure equilibration. a) Choline Chloride, b) Acetylcholine Chloride, c) Tetraethylammonium Chloride, d) Tetrapropylammonium Bromide

show small current evolution and strikingly similar features in the reverse scan and its position seems to be correlated to the halide anion of the QAS. When both HBDs are paired with ChCl, peaks at approximately 0.5 V are present. These same peaks can also be identified when AcChCl or TEAC are used as the QAS. On the other hand, when TPAB is used as the QAS, both peaks are shifted by almost -0.5 V . By varying the QAS, we see that the features that result in the CV can be heavily tied to the structure of these HBD, with both being primarily carboxylic acids and containing a phenol group. Comparisons between amide-based DES (Figure 13), such as urea and acetamide, paired with ChCl and AcChCl show peaks occurring at substantially negative potentials ($-1.5\text{ V vs. Ag/AgCl}$). Samples containing urea also show a feature around 0 V , which is also present in the N, N'-dimethylurea samples (Figure S9), whereas the acetamide DES shows a flatter curve in the reverse scan. Once again, changing the QAS's cation structure does not seem to influence the features present on the CV. However, the halide species in the QAS does. In fact, the TPAB samples paired with acetamide only show the feature at $-0.5V$, Figure S7. This can also be observed for N, N'-dimethylurea. Unfortunately, combinations between the bromine based QAS and urea did not result in liquid samples at room temperature and therefore it was not possible to characterize them electrochemically.

Again, alcohol/polyol-based DES such as ethylene glycol (Figure S8) and glycerol (Figure 14) seem to follow the same trend indicated above, where the feature of the reverse scan seems

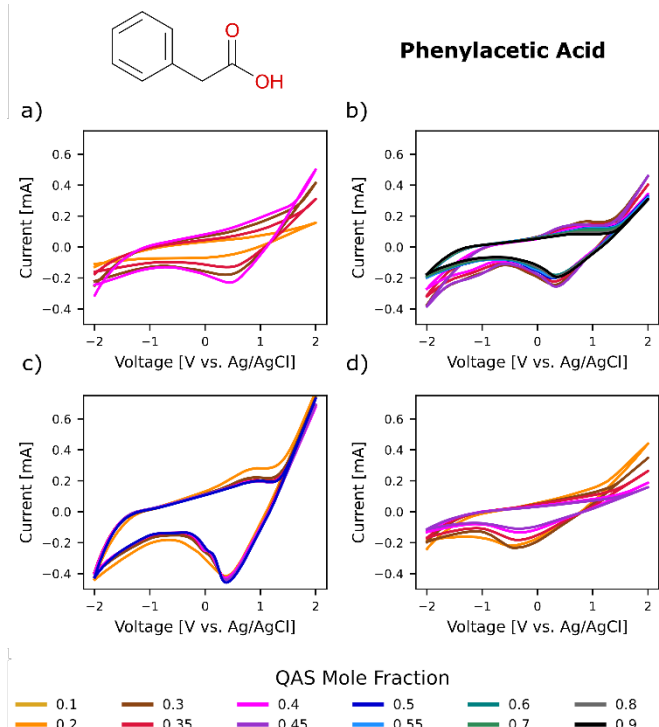


Figure 11 Cyclic voltammograms of phenylacetic acid-based DES as a function of QAS mole fraction. For all measurement, the potential was varied from $-2V$ and $2V$ with a scan rate of 100 mV/s and a total of 4 cycles per sample to ensure equilibration. a) Choline Chloride, b) Acetylcholine Chloride, c) Tetraethylammonium Chloride, d) Tetrapropylammonium Bromide

to be tied to the nature of the halide component on the ammonium salt and the molecular structure of the HBD.

It seems that varying the halide of the QAS has an effect on shifting peak positions. However, it is noted for other studies involving ChCl based DES that the positive limits of the CV is a result of the oxidation of Cl^- ions.^{73,74} In fact, for all samples containing Br^- , the onset of the limiting potential in the forward scan shifts towards smaller potential, further confirming that the limiting processes are tied to the change in oxidation state the halide anion in the QAS species. However, the negative limiting potentials may be more closely influenced by the nature of the HBD. Finally, another interesting feature of the CV data is the variation in the slope of the limiting processes (e.g., see Figure 14). This quantity seems to be changing with the molar composition of the DES samples. We extracted the slope at both Anodic and Cathodic limits and, when plotting against the QAS mole fraction, noticed that the data follow the same trend as for conductivity, Figure S12-S15. The similarity between the data suggests that the limiting processes of the cyclic voltammetry are conductance limited. Even though the CV data shows features in its reverse scan, these can be avoided by reducing the upper limit of the voltage range in the measurement itself. This change was not implemented in this study as maintaining the same CV parameters was important to allow for parallel and high-throughput measurements between different DES sample conditions and compositions.

Looking at the combined experimental results, we start to notice some trends. Samples containing AcChCl as their QAS

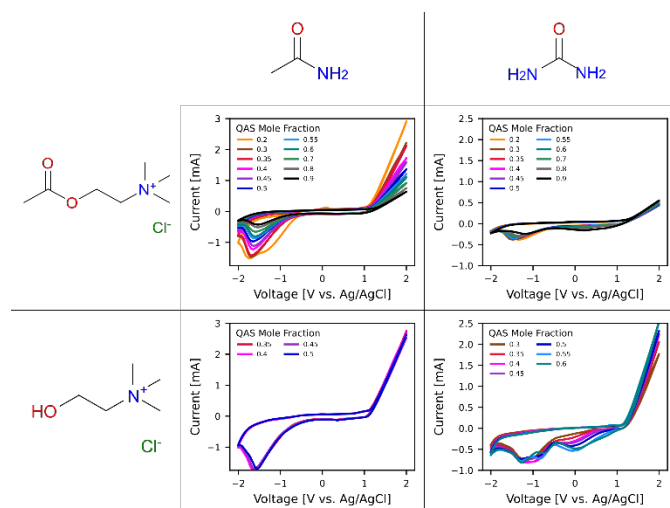


Figure 13 Comparison between the cyclic voltammograms of Acetamide (Left) and Urea (Right) in their combinations with Acetylcholine Chloride (Top) and Choline Chloride (Bottom). The two HBD have similar molecular structure and it is possible to show parallel between the CV features in the backward scan. The two QAS both have Chlorine as their halide anion and show similarities in their voltammograms

show a very low melting point and most were found to be liquid at room temperature (19 – 24 °C). Even though ChCl has a smaller cation structure, the addition of the acetyl functional group increases the asymmetry of the cation species and decreases the melting point of the salt (i.e., 146 – 150 °C, compared to 302 °C for ChCl).^{75,76} This confirms that, for pure species with lower melting temperatures, the resulting DES are more likely to be liquid at lower temperatures. Yet even though TPAB melts at 270 °C, it has a very limited number of liquid samples when compared to those formulated using ChCl or TEAC, in spite of their higher melting points. This could be attributed to the influence of the Br^- anion.^{77,78} In fact, it is known that DES form a complex solvation environment where, for Type III DES, the strongest interactions are between the halide species and the hydrogen bonding sites of both the HBD and the cation species of the QAS.^{2,79} This can help explain why changing the halide from chlorine to iodine, while maintaining the cation structure intact, did not produce any liquid samples at room temperature.

In this study, we also show that for certain combinations of DES precursor materials there can be a wide range of compositions that yield liquid samples at room temperature. While some of the measured electrochemical properties seem to not change with respect to the composition of the sample (i.e., potential window), others have a stronger relationship to the ratio of QAS/HBD and the molecular structure of the species. For example, we demonstrate that electrolytes are electrochemically limited by viscosity, both in the conductivity and in the limiting processes on the CV. However, for the same combination of QAS and HBD, there are several samples which exhibit high conductivities, broad potential window and show electrochemical stability. This further motivates their potential use in energy-related applications, such as batteries electrolytes. Moreover, as we have demonstrated in this study,

it is important to also study DES systems outside of their eutectic point as it can help to understand the complex relationships between molecular structures, solvation, and transport coefficients (i.e., viscosity, diffusivity). This will also allow us to build better predictive models for DES materials, and to advance their design and application as green solvents. In fact, there are likely practical situations in which more favorable properties exist at compositions that fall outside of the eutectic point. Without more comprehensive studies of DES materials, advancement and practical applications will be hindered. The traditional route for the formulation of these solvents is prohibitively slow and cumbersome to study their vast molecular design space. Thus, data-driven design of experiments, coupled with high-throughput workflows for synthesis and characterization are essential for their advancement. The results from the current and any subsequent experimental campaigns will also be integrated in the selection of new molecules, moving the workflow towards a closed-loop system. This strategy could be used to both validate the initial selection of candidate molecules, as well as to build a more diverse and complete database of DES properties. Future work will focus on generating predictive Quantitative Structure-Property Relationship (QSPR) models to better understand which molecular features lead to ideal DES properties, as seen in Halder et al.⁸⁰ This will in turn allow for the integration of AI-driven algorithms to aid in the exploration of new combinations of QASs and HBDs that could lead to mixture with the desired

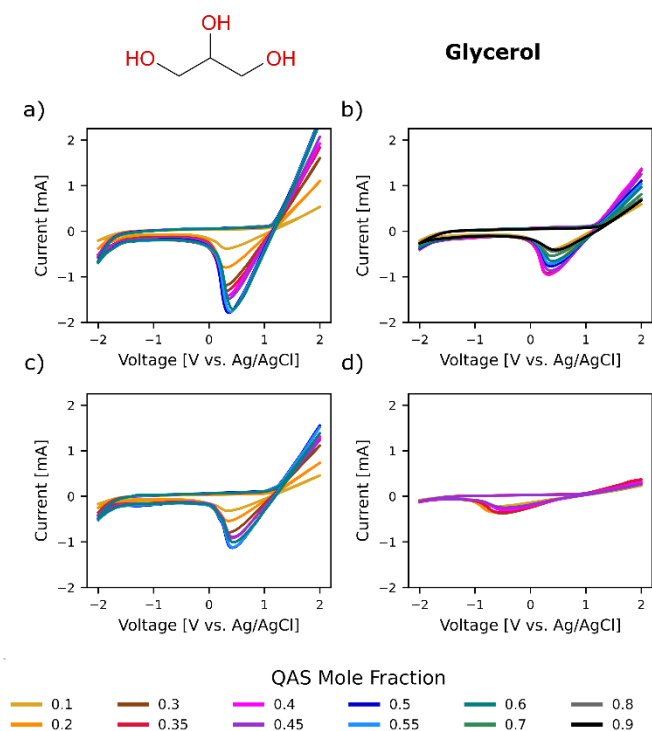


Figure 14 Cyclic voltammograms of Glycerol-based DES as a function of QAS mole fraction. For all measurement, the potential was varied from –2V and 2V with a scan rate of 100 mV/s and a total of 4 cycles per sample to ensure equilibration. The position of the feature on the backward scan seems to be dependent on the halide anion of the QAS component. a) Choline Chloride, b) Acetylcholine Chloride, c) Tetraethylammonium Chloride, d) Tetrapropylammonium Bromide

properties, in this case for use as electrolytes in redox flow batteries. Moreover, redox-active organic molecules will also be integrated in the DES campaign, both in a binary and ternary composition, to aid in the design of anolyte and catholyte solutions for use in RFBs.

Finally, while the cheminformatic approach towards outlining the design space is not optimized and still in an infant stage, its importance in serving as a steppingstone for the rest of this work and future work should be noted. The implemented single-objective approach was selected to demonstrate the implementation of high-throughput workflows for the synthesis and study of multivariate design spaces. However, before it is possible to close the loop and build a fully automated system for the exploration of the DES design space, it is crucial to promote more accessible automation infrastructures based on open-science principles to encourage transparency and reproducibility of protocols and results. This would allow an increase in the diversity of data available on DES and allow further advancements in the predictive models for this class of materials. Luckily, these data-driven strategies can be easily adapted to use multicriteria decision approaches, exploit the information learned from these high-throughput experimental campaigns to propose new candidate molecules more readily and accurately for the targeted application.

Conclusions

The use of DES as electrolytes for RFBs is attractive due to their low-cost, green environmental footprint, wide potential window, and adequate ionic conductivity. Despite these benefits, identifying optimal DES is challenging due to the massive molecular design space that is associated with these materials. High-throughput and data-driven strategies, such as those presented here, provide an avenue towards developing DES electrolytes designed specifically for target applications (e.g., RFB). We demonstrated the use of cheminformatics to outline experimental designs that balance benefits from analyzing diverse chemical precursors with the engineering constraints that are associated to the intended end-use. DES were then synthesized in high-throughput, to complete an experimental campaign spanning 50 QAS/HBD combinations and 12 molar ratios for a total of 600 unique samples. The systematic characterization of such a large number of DES-candidates is valuable and unique in the current literature, where data on DES electrolytes is still scarce and overwhelmingly focused on choline chloride samples. Importantly, the high-throughput electrochemical characterization reported in this work also identified several promising electrolyte candidates with wide electrochemical potential windows (over 3 V) and ionic conductivities above 1 mS/cm. This suggests that there are likely numerous promising electrolyte materials within the vast molecular design space of DES that remain to be discovered.

While efforts to move this work closer towards an automated closed loop system are underway, the methods outlined in this study could quickly increase the DES data that is available and openly shared for use with advanced statistical

methods, such as quantitative structure property relationships (QSPR). The use of advanced methods to predict DES properties from molecular features and formulation parameters will become essential elements in future investigations aiming to efficiently sample DES candidates. In addition, methods outlined in this study can also be extended beyond the analysis of DES-based electrolytes and can perhaps provide some inspiration for approaching other materials design problems with large design spaces. The proposed workflow could be used to study other systems where the thermodynamics of mixtures play an important role such as microemulsions, especially for drug delivery applications, or the phase transition temperature of lipid systems. Embracing these data-driven strategies and the use of low-cost, automatic, and open-source robotic systems will make the incorporation of AI-driven algorithms and iterative exploratory campaigns into the design of experiments (DOE) much more accessible to the scientific community. This will allow to more efficiently arrive at new knowledge that will facilitate the design of DES electrolytes with optimum properties or other multivariate material design spaces.

Author Contributions

LP, SA, and DB supervised the project development and are responsible for the project conceptualization. JR and LP developed the high-throughput experimental and software methodology. JR conducted and completed the cheminformatic campaign and its data visualization stages. JR and MP completed the formal experimental investigation and conducted the formal analysis of the collected experimental data. MP completed the data visualization and software developed for this project. JR and MP completed the original draft of the manuscript and MP curated the review and editing for its final version. LP, SA and DB provided feedback and edits to the manuscript.

Conflicts of interest

The authors declare no competing financial interest.

Acknowledgements

This project was supported by: National Science Foundation through NSF-CBET grant no. 1917340, the Data Intensive Research Enabling Clean Technology (DIRECT) National Science Foundation (NSF) National Research Traineeship (DGE-1633216), and the UW Molecular Engineering Materials Center, a Materials Research Science and Engineering Center (Grant No. DMR-1719797). We acknowledge the State of Washington through the University of Washington (UW) Clean Energy Institute and the UW eScience Institute. Testing of this work was conducted in facilities supported by the University of Washington Department of Chemical Engineering.

Notes and reference

1. Martins, M. A. R., Pinho, S. P. & Coutinho, J. A. P. Insights into the Nature of Eutectic and Deep Eutectic Mixtures. *Journal of Solution Chemistry* **48**, 962–982 (2019).
2. Smith, E. L., Abbott, A. P. & Ryder, K. S. Deep Eutectic Solvents (DESs) and Their Applications. *Chemical Reviews* **114**, 11060–11082 (2014).
3. Zhang, Q., De Oliveira Vigier, K., Royer, S. & Jérôme, R. Deep eutectic solvents: Syntheses, properties and applications. *Chemical Society Reviews* **41**, 7108–7146 (2012).
4. Smith, E. L., Abbott, A. P. & Ryder, K. S. Deep Eutectic Solvents (DESs) and Their Applications. *Chemical Reviews* **114**, 11060–11082 (2014).
5. Bahadori, L., Boyd, R., Warrington, A., Shafeeyan, M. S. & Nockemann, P. Evaluation of ionic liquids as electrolytes for vanadium redox flow batteries. *Journal of Molecular Liquids* **317**, 114017 (2020).
6. Chakrabarti, B. *et al.* Evaluation of a non-aqueous vanadium redox flow battery using a deep eutectic solvent and graphene-modified carbon electrodes via electrophoretic deposition. *Batteries* **6**, 1–20 (2020).
7. Ejigu, A., Greatorex-Davies, P. A. & Walsh, D. A. Room temperature ionic liquid electrolytes for redox flow batteries. *Electrochemistry Communications* **54**, 55–59 (2015).
8. Cao, X., Wang, S. & Xue, X. A Zn–Ce Redox Flow Battery with Ethaline Deep Eutectic Solvent. *ChemSusChem* **14**, 1747–1755 (2021).
9. Xu, Q. *et al.* A deep eutectic solvent (DES) electrolyte-based vanadium-iron redox flow battery enabling higher specific capacity and improved thermal stability. *Electrochimica Acta* **293**, 426–431 (2019).
10. Chakrabarti, M. H. *et al.* Prospects of applying ionic liquids and deep eutectic solvents for renewable energy storage by means of redox flow batteries. *Renewable and Sustainable Energy Reviews* **30**, 254–270 (2014).
11. Ortiz-Martínez, V. M., Gómez-Coma, L., Pérez, G., Ortiz, A. & Ortiz, I. The roles of ionic liquids as new electrolytes in redox flow batteries. (2020) doi:10.1016/j.seppur.2020.117436.
12. Darling, R. M., Gallagher, K. G., Kowalski, J. A., Ha, S. & Brushett, F. R. Pathways to low-cost electrochemical energy storage: A comparison of aqueous and nonaqueous flow batteries. *Energy and Environmental Science* **7**, 3459–3477 (2014).
13. Dmello, R., Milshtein, J. D., Brushett, F. R. & Smith, K. C. Cost-driven materials selection criteria for redox flow battery electrolytes. *Journal of Power Sources* (2016) doi:10.1016/j.jpowsour.2016.08.129.
14. Alotto, P., Guarnieri, M. & Moro, F. Redox flow batteries for the storage of renewable energy: A review. *Renewable and Sustainable Energy Reviews* **29**, 325–335 (2014).
15. Cruz, H., Jordão, N. & Branco, L. C. Deep eutectic solvents (DESs) as low-cost and green electrolytes for electrochromic devices. *Green Chemistry* **19**, 1653–1658 (2017).
16. Goeltz, J. C. & Matsushima, L. N. Metal-free redox active deep eutectic solvents. *Chemical Communications* **53**, 9983–9985 (2017).
17. Sinclair, N. S., Poe, D., Savinell, R. F., Maginn, E. J. & Wainright, J. S. A Nitroxide Containing Organic Molecule in a Deep Eutectic Solvent for Flow Battery Applications. *Journal of The Electrochemical Society* **168**, 020527 (2021).
18. Holbrey, J. D ; Seddon, K. R. Ionic Liquids. *Clean Technol. Environ. Policy* **1**, 223–236 (1999).
19. Kaul, M. J., Qadah, D., Mandella, V. & Dietz, M. L. Systematic evaluation of hydrophobic deep-

- melting eutectics as alternative solvents for the extraction of organic solutes from aqueous solution. *RSC Advances* **9**, 15798–15804 (2019).
20. Haghbakhsh, R., Parvaneh, K., Raeissi, S. & Shariati, A. A general viscosity model for deep eutectic solvents: The free volume theory coupled with association equations of state. *Fluid Phase Equilibria* **470**, 193–202 (2018).
21. Lloret, J. O., Vega, L. F. & Llovel, F. Accurate description of thermophysical properties of Tetraalkylammonium Chloride Deep Eutectic Solvents with the soft-SAFT equation of state. *Fluid Phase Equilibria* **448**, 81–93 (2017).
22. González De Castilla, A., Bittner, J. P., Müller, S., Jakobtorweihen, S. & Smirnova, I. Thermodynamic and Transport Properties Modeling of Deep Eutectic Solvents: A Review on gE-Models, Equations of State, and Molecular Dynamics. *Journal of Chemical and Engineering Data* **65**, 943–967 (2020).
23. Dean, W., Klein, J. & Gurkan, B. Do Deep Eutectic Solvents Behave Like Ionic Liquid Electrolytes? A Perspective from the Electrode-Electrolyte Interface. *Journal of The Electrochemical Society* **168**, 026503 (2021).
24. Matsuda, S., Nishioka, K. & Nakanishi, S. High-throughput combinatorial screening of multi-component electrolyte additives to improve the performance of Li metal secondary batteries. *Scientific Reports* **9**, 1–3 (2019).
25. Cheng, L. *et al.* Accelerating Electrolyte Discovery for Energy Storage with High-Throughput Screening. *Journal of Physical Chemistry Letters* vol. 6 283–291 (2015).
26. Sun, S. *et al.* Accelerated Development of Perovskite-Inspired Materials via High-Throughput Synthesis and Machine-Learning Diagnosis. *Joule* **3**, 1437–1451 (2019).
27. Whitacre, J. F. *et al.* An Autonomous Electrochemical Test Stand for Machine Learning Informed Electrolyte Optimization. *Journal of The Electrochemical Society* **166**, A4181 (2019).
28. Cummins, D. J. & Bell, M. A. Integrating Everything: The Molecule Selection Toolkit, a System for Compound Prioritization in Drug Discovery. *J. Med. Chem* **59**, 7010 (2016).
29. Nicolaou, C. A. & Brown, N. Multi-objective optimization methods in drug design. *Drug Discovery Today: Technologies* **10**, (2013).
30. Cruz-Monteagudo, M., Borges, F. & Cordeiro, M. N. D. S. Desirability-Based Multiobjective Optimization for Global QSAR Studies: Application to the Design of Novel NSAIDs with Improved Analgesic, Antiinflammatory, and Ulcerogenic Profiles. (2008) doi:10.1002/jcc.20994.
31. pozzo-research-group. Automation-Hardware: Pozzo Group OT2 Hardware. *GitHub* <https://github.com/porzo-research-group/Automation-Hardware> (2021).
32. Ibrahim, R. K. *et al.* Physical properties of ethylene glycol-based deep eutectic solvents. *Journal of Molecular Liquids* **276**, 794–800 (2019).
33. Gurkan, B., Squire, H. & Pentzer, E. Metal-Free Deep Eutectic Solvents: Preparation, Physical Properties, and Significance. *Journal of Physical Chemistry Letters* **10**, 7956–7964 (2019).
34. Rodriguez, J. *et al.* PhasIR: An Instrumentation and Analysis Software for High-throughput Phase Transition Temperature Measurements. *Journal of Open Hardware* **5**, (2021).
35. Politi, M. & Rodriguez, J. phasIR: Python modules for high-throughput measurement of melting point using IR bolometry. *GitHub*

- <https://github.com/pozzo-research-group/phasIR> (2021).
36. Dave, A. *et al.* Autonomous discovery of battery electrolytes with robotic experimentation and machine-learning. *arXiv* (2019) doi:10.1016/j.xcrp.2020.100264.
37. Murbach, M. D., Gerwe, B., Dawson-Elli, N. & Tsui, L.-K. impedance.py: A Python package for electrochemical impedance analysis. doi:10.21105/joss.02349.
38. Murray, P. M. & Forfar, L. C. The Application of Advanced Design of Experiments for the Efficient Development of Chemical Processes. *Chemical Informatics* **03**, (2017).
39. Cao, B. *et al.* How to optimize materials and devices via design of experiments and machine learning: Demonstration using organic photovoltaics. *ACS Nano* vol. 12 7434–7444 (2018).
40. Kazakov, A. , Magee, J. , Chirico, R. , Diky, V. , Kroenlein, K. , Muzny, C. and Frenkel, M. Ionic Liquids Database - ILThermo (v2.0). *NIST* (2013).
41. Marcus, Y. *Deep Eutectic Solvents*. *Deep Eutectic Solvents* (Springer International Publishing, 2019). doi:10.1007/978-3-030-00608-2.
42. Swain, M. PubChemPy. (2014).
43. Kim, S., Thiessen, P. A., Cheng, T., Yu, B. & Bolton, E. E. An update on PUG-REST: RESTful interface for programmatic access to PubChem. *Nucleic Acids Research* **46**, W563–W570 (2018).
44. Kim, S. *et al.* Pug-View: Programmatic access to chemical annotations integrated in PubChem. *Journal of Cheminformatics* **11**, 56 (2019).
45. Cereto-Massagué, A. *et al.* Molecular fingerprint similarity search in virtual screening. *Methods* **71**, 58–63 (2015).
46. National Institute of Health. PubChem Substructure Fingerprint. (2009).
47. Bajusz, D., Rácz, A. & Héberger, K. Why is Tanimoto index an appropriate choice for fingerprint-based similarity calculations? *Journal of Cheminformatics* **7**, 1–13 (2015).
48. Morgan, H. L. The Generation of a Unique Machine Description for Chemical Structures-A Technique Developed at Chemical Abstracts Service. *American Chemical Society* **5**, 107–113 (1965).
49. Firdaus Begam, B., Begam, B. F. & Kumar, J. S. Visualization of Chemical Space Using Principal Component Analysis. *World Applied Sciences Journal* **29**, 53–59 (2014).
50. Ivosev, G., Burton, L. & Bonner, R. Dimensionality reduction and visualization in principal component analysis. *Analytical Chemistry* **80**, 4933–4944 (2008).
51. Verslycke, T. *et al.* The Chemistry Scoring Index (CSI): A hazard-based scoring and ranking tool for chemicals and products used in the oil and gas industry. *Sustainability (Switzerland)* **6**, 3993–4009 (2014).
52. Dehghan-Manshadi, B., Mahmudi, H., Abedian, A. & Mahmudi, R. A novel method for materials selection in mechanical design: Combination of non-linear normalization and a modified digital logic method. *Materials and Design* **28**, 8–15 (2007).
53. Spiwok, V. & Kříž, P. Time-Lagged t-Distributed Stochastic Neighbor Embedding (t-SNE) of Molecular Simulation Trajectories. *Frontiers in Molecular Biosciences* **7**, 132 (2020).
54. Janssen, A. P. A. *et al.* Drug Discovery Maps, a Machine Learning Model That Visualizes and Predicts Kinome-Inhibitor Interaction Landscapes. *Journal of Chemical Information and Modeling* **59**, 1221–1229 (2019).

ARTICLE

Journal Name

55. Maugeri, Z. & Domínguez De María, P. Novel choline-chloride-based deep-eutectic-solvents with renewable hydrogen bond donors: Levulinic acid and sugar-based polyols. *RSC Advances* **2**, 421–425 (2012).
56. Abbott, A. P., Capper, G., Davies, D. L., Rasheed, R. K. & Tambyrajah, V. Novel solvent properties of choline chloride/urea mixtures. *Chemical Communications* 70–71 (2003) doi:10.1039/b210714g.
57. Abbott, A. P. *et al.* Glycerol eutectics as sustainable solvent systems. *Green Chemistry* **13**, 82–90 (2011).
58. Shahbaz, K., Mjalli, F. S., Hashim, M. A. & Al Nashef, I. M. Using deep eutectic solvents for the removal of glycerol from palm oil-based biodiesel. *Journal of Applied Sciences* vol. 10 3349–3354 (2010).
59. Abbott, A. P., Boothby, D., Capper, G., Davies, D. L. & Rasheed, R. K. Deep Eutectic Solvents formed between choline chloride and carboxylic acids: Versatile alternatives to ionic liquids. *J Am Chem Soc* **126**, 9142–9147 (2004).
60. `scipy.signal.find_peaks`. https://docs.scipy.org/doc/scipy/reference/generated/scipy.signal.find_peaks.html.
61. Abbott, A. P., Capper, G., Davies, D. L., Rasheed, R. K. & Tambyrajah, V. Novel solvent properties of choline chloride/urea mixtures †. (2002) doi:10.1039/b210714g.
62. Biernacki, K., Souza, H. K. S., Almeida, C. M. R., Magalhães, A. L. & Gonçalves, M. P. Physicochemical Properties of Choline Chloride-Based Deep Eutectic Solvents with Polyols: An Experimental and Theoretical Investigation. *ACS Sustainable Chemistry and Engineering* **8**, 18712–18728 (2020).
63. Hou, Y. *et al.* Novel binary eutectic mixtures based on imidazole. *Journal of Molecular Liquids* **143**, 154–159 (2008).
64. F.S. Ghareh Bagh, K. Shahbaz, F.S. Mjalli, I.M. AlNashef, M. A. H. Electrical conductivity of ammonium and phosphonium based deep eutectic solvents: Measurements and artificial intelligence-based prediction | Elsevier Enhanced Reader. *Fluid Phase Equilibria* **356**, 30–37 (2013).
65. Abbott, A. P., Harris, R. C. & Ryder, K. S. Application of hole theory to define ionic liquids by their transport properties. *Journal of Physical Chemistry B* **111**, 4910–4913 (2007).
66. López, N., Delso, I., Matute, D., Lafuente, C. & Artal, M. Characterization of xylitol or citric acid:choline chloride:water mixtures: Structure, thermophysical properties, and quercetin solubility. *Food Chemistry* **306**, (2020).
67. Abbott, A. P., Harris, R. C. & Ryder, K. S. Application of hole theory to define ionic liquids by their transport properties. *Journal of Physical Chemistry B* **111**, 4910–4913 (2007).
68. García, G., Aparicio, S., Ullah, R. & Atilhan, M. Deep eutectic solvents: Physicochemical properties and gas separation applications. *Energy and Fuels* **29**, 2616–2644 (2015).
69. Chalamala, B. R. *et al.* Redox flow batteries: An engineering perspective. *Proceedings of the IEEE* **102**, 976–999 (2014).
70. Li, Q. *et al.* The electrochemical stability of ionic liquids and deep eutectic solvents. *Science China Chemistry* **59**, 571–577 (2016).
71. Bahadori, L. *et al.* Physicochemical properties of ammonium-based deep eutectic solvents and their electrochemical evaluation using organometallic reference redox systems. *Electrochimica Acta* **113**, 205–211 (2013).

72. Li, Q. *et al.* The electrochemical stability of ionic liquids and deep eutectic solvents. *Science China Chemistry* **59**, 571–577 (2016).
73. Haerens, K., Matthijs, E., Binnemans, K. & Van Der Bruggen, B. Electrochemical decomposition of choline chloride based ionic liquid analogues. (2009) doi:10.1039/b906318h.
74. Fuchs, D. *et al.* Electrochemical Behavior of Graphene in a Deep Eutectic Solvent. *Cite This: ACS Appl. Mater. Interfaces* **12**, 40948 (2020).
75. Sigma-Aldrich. Acetylcholine Chloride; SDS A6625. 1–8 (2021).
76. Acros-Organics. Choline Chloride ; SDS AC110290000. 1–7 (2021).
77. Sigma-Aldrich. Tetraethylammonium Chloride ; SDS T2265. 1–9 (2021).
78. Sigma-Aldrich. Tetrapropylammonium Bromide; SDS 225568. 1–8 (2020).
79. Zhang, Y. *et al.* Liquid Structure and Transport Properties of the Deep Eutectic Solvent Ethaline. *J. Phys. Chem. B* **124**, 2021 (2020).
80. Halder, A. K., Ambure, P., Perez-Castillo, Y. & Cordeiro, M. N. D. S. Turning deep-eutectic solvents into value-added products for CO₂ capture: A desirability-based virtual screening study. *Journal of CO₂ Utilization* **58**, 101926 (2022).